Journal Pre-proof

Characterization and source apportionment of black carbon aerosol in the Nanjing Jiangbei New Area based on two years of measurements from Aethalometer

Sihan Xiao, Xingna Yu, Bin Zhu, K. Raghavendra Kumar, Mei Li, Lei Li

PII: S0021-8502(19)30565-8

DOI: https://doi.org/10.1016/j.jaerosci.2019.105461

Reference: AS 105461

To appear in: *Journal of Aerosol Science*

Received Date: 2 January 2019

Revised Date: 3 July 2019

Accepted Date: 24 September 2019

Please cite this article as: Xiao S, Yu X, Zhu B, Kumar KR, Li M, Li L, Characterization and source apportionment of black carbon aerosol in the Nanjing Jiangbei New Area based on two years of measurements from Aethalometer, *Journal of Aerosol Science*, https://doi.org/10.1016/j.jaerosci.2019.105461.

Characterization and source apportionment of black carbon aerosol in the Nanjing Jiangbei New Area based on two years of measurements from Aethalometer

Sihan Xiao[a, b], Xingna Yu[a*], Bin Zhu[a], K. Raghavendra Kumar[a], Mei Li[c, d], Lei Li[d, e]

[a]*Collaborative Innovation Centre on Forecast and Evaluation of Meteorological Disasters, Key Laboratory of Meteorological Disaster, Ministry of Education (KLME), International Joint Laboratory on Climate and Environment Change (ILCEC), Key Laboratory for Aerosol-Cloud-Precipitation of China Meteorological Administration, School of Atmospheric Physics, Nanjing University of Information Science and Technology, Nanjing 210044, China*

[b]*Shaoyang Meteorological Bureau, Shaoyang 422000, China*

[c]*Kunshan Hexin Mass Spectrometry Technology Co., Ltd, Kunshan 215311, China*

[d]*Institute of Mass Spectrometer and Atmospheric Environment, Jinan University, Guangzhou 510632, China*

[e]*Guangzhou Hexin Mass Spectrometry Technology Co., Ltd, Guangzhou 510530, China*

***Corresponding author**

Email: xnyu@nuist.edu.cn (Prof. Dr. Xingna Yu)

Abstract

Black carbon (BC) aerosols were measured using a seven channel Aethalometer at a suburban site of Nanjing, East China from January 2015 to December 2016 to study its temporal variations and quantify the magnitude of BC from fossil fuel (BC_{ff}) and biomass burning (BC_{bb}) sources. The mean BC mass concentration was observed to be 2200 ± 1309 ng/m^3 at the sampling site during the entire observation period, with the highest (lowest) concentrations found in the winter (summer and spring). A distinct diurnal variations in BC revealed with two maximum peaks occurred between 06:00 and 09:00 local time (LT) and 19:00 and 22:00 LT in all four seasons, was correlated with source emissions, meteorology, and dynamics of the atmospheric boundary layer. A significant seasonality was observed in the absorption Ångström exponent (α) with higher in spring and winter seasons, and lower during the summer. Further, it is evident that the contribution of BC_{ff} (BC_{ff}%) dominated during the observation period with the mean contributions of BC_{ff} % and BC_{bb}% to the BC were found to be ~81% and 19%, respectively. Similar to α, BC_{bb}% also exhibited high fractions in spring and winter suggests an enhanced contribution from biomass burning sources, and a low in summer. The results from both the potential source contribution function (PSCF) and concentration weighted trajectory (CWT) models indicated that the air masses originating from the northern Zhejiang and Anhui provinces were the potential source areas responsible for the high BC concentrations attributed from agricultural waste burning in Nanjing.

Keywords: Aethalometer; Black carbon aerosol; Absorption Ångström exponent; Source apportionment; Nanjing.

1. Introduction

Atmospheric aerosols have an important influence on the radiation balance of the earth-atmosphere system, both at regional and even global scales (Ramanathan and Carmichael, 2008). The carbonaceous aerosol is one of the most important components of aerosol particles, which are mainly composed of organic carbon (OC) and black carbon (BC) (Bisht et al., 2015; Begam et al., 2016; Prasad et al., 2018). Black carbon aerosols are often produced by human activities, resulting from the incomplete combustion of fossil fuels and biomass (Ravi Kiran et al., 2018). Considering the key role that BC plays in atmospheric radiative effects, as well as health effects, BC aerosols have become an important topic in the recent years. However, BC can heat the atmosphere and contribute strikingly to global warming because of its strong absorption of incoming solar radiation from the visible to infrared wavelengths. Some studies have shown that BC may be the second greatest contributor to the greenhouse effect after CO_2 (Babu and Moorthy, 2002; Joshi et al., 2016; Liu et al., 2018). Furthermore, it contributes greatly to indirect radiative forcing by acting as cloud condensation nuclei (Dumka et al., 2010; Joshi et al., 2016). BC can also reside in the atmosphere from 1 week to 10 days in the absence of precipitation (Kumar et al., 2011; Tiwari et al., 2013), thereby facilitating the deterioration of air quality (Liu et al., 2018). Being nearly in the sub-micron size range, BC particles are readily able to penetrate into the human respiratory system and cause adverse effects on health (Babu and Moorthy, 2002).

It is well known that a tremendous amount of pollutants have been emitted in East Asia due to rapid industrial development, surging auto possession, and frequent amount of seasonal biomass burning (Pan et al., 2011; Liu et al., 2018; Kolhe et al., 2019). Based on the study of regional and global BC emission inventories, approximately 1/4 of the global annual BC emissions were found to be derived from China (Bond, 2004; Zha et al., 2014), However, the contribution of different source types to BC aerosol remains unclear due to their heterogeneous emission sources and strengths (Pan et al., 2011; Prasad et al., 2018). Since the 1990s, field measurements of BC aerosols in China have been performed in many cities, including those in the

Pearl River Delta region (Cheng et al., 2006; Huang et al., 2012; Tan et al., 2016), Yangtze River Delta region (Feng et al., 2014; Zhang et al., 2015; Zhuang et al., 2014), and the Beijing-Tianjin-Hebei region (Ran et al., 2016; Yan et al. 2008). These studies have provided useful information for better comprehending the characteristics of BC aerosols in China. However, most studies relied on the short-term measurements, and few studies have attempted to estimate the contribution of BC sources due to fossil fuel and biomass burning.

Nanjing is an economic megacity in the Yangtze River Delta (YRD) region, which is confronted with severe air pollution (An et al., 2014). In this study, measurements of BC aerosol were conducted from January 2015 to December 2016 with a seven channel Aethalometer. The data obtained is used to investigate the temporal variations of BC mass concentrations on daily, monthly, and seasonal scales, and identify potential source areas of BC through the Potential Source Contribution Function (PSCF) and Concentration Weighted Trajectory (CWT) statistical models. Further, we also investigated to quantify the BC mass concentration in terms of BC from fossil fuel (BC_{ff}) and biomass burning (BC_{bb}) sources using an Aethalometer model. The results may aid in our understanding of the pollution characteristics of BC and provide useful information with implications for formulating BC emissions inventory over Nanjing in the YRD region, East China.

2. Materials and methods

2.1. Sampling site

Measurements of BC were performed on the campus of Nanjing University of Information Science and Technology (32°21’N, 118°72’E), a suburban site of Nanjing in the Jiangbei New Area (Fig. 1). The Jiangbei New Area is the only state-level new district in East China located within the Jiangsu Province (Figure S1 of Supplementary Material (SM)). It is located north of the Yangtze River in Nanjing, with a total area of approximately 2451 km^2, and accounting for 37% of the Nanjing area. It is also an important node of the Yangtze River Economic Belt. The pollution sources in this area are primarily emissions from traffic emissions, urban building and road constructions, and industrial activities (Wang et al., 2016). The Nanjing chemical

industry is situated ~3 km northeast of the sampling site; there were also iron and steel plants within 2 km of the site and main roads ~ 500 m near to the sampling site. General meteorological parameters were monitored continuously by the automatic weather station (AWS) installed on the campus, which is approximately 800 m away from the measurement site.

2.2. Instrumentation

Mass concentrations of BC aerosol were recorded with an Aethalometer (Model AE-33, Magee Scientific Company, USA) at 370 nm, 470 nm, 525 nm, 590 nm, 660 nm, 880 nm, and 940 nm. The Aethalometer was placed in an air-conditioned room, on the roof of the Meteorology Building located on the campus of Nanjing University of Information Science and Technology, Nanjing where the temperature inside of the room was maintained at 25ºC. The instrument aspirates ambient air through an inlet tube mounted vertically, at an elevation of 2 m from the roof level and ~30 m from the ground level. The particles in the incoming air flow were deposited on the quartz filter tape of the Aethalometer and the BC concentration was determined by measuring the change in transmittance through the quartz filter. The instrument continuously operated at a constant flow rate of 5.0 litres/min (LPM), with a measurement frequency of 5 min. A 2.5 μm sharp cut-point of the cyclone was used at the inlet of the sampling tube to avoid dust and other coarse particles entering the instrument. After passing through the inlet, the sampled air was then dried by a drier to control the relative humidity (RH) to ~40%. Further details of the instrument and its operation have been discussed elsewhere (Hansen et al., 1984). The light absorption measured at 880 nm is considered to represent the effect of BC, since BC is the principal absorber of light at that wavelength, while other known aerosol components have negligible absorption (Bodhaine, 1995). An absorption efficiency value of 16.6 m^2 g^{-1} (given by manufacturer) was used to determine the BC mass concentration at 880 nm as used by previous authors (Beegum et al., 2009; Kumar et al., 2011; Begam et al., 2016; Liu et al., 2018; Prasad et al., 2018). Periodical and routine calibration, and flow check of the instrument were carried out to maintain the data reliability and precision.

The Aethalometer calculated the absorption coefficients by measuring the attenuation (ATN) of the incident light due to which the particles impinged on the tetrafluoroethylene (TFE)-coated glass filter, and the BC concentration was determined using the wavelength-dependent mass absorption cross section (Ran et al., 2016). Because the Aethalometer relies on filter sampling, several systematic errors exist in the measurement of BC. It has been observed that after the complete advancement of filter tape, the deposition of BC particles started impinging on the filter tape and the loading apparently increases with the realt-time (Hansen et al., 1984; Begam et al., 2016). Consequently, the relationship between BC loading and ATN change is non-linear, and this results in the underestimation of BC concentrations, with is referred to as the "loading effect"(Virkkula et al., 2007; Beegum et al., 2009; Singh et al., 2015; Begam et al., 2016; Vaishya et al., 2017; Ravi Kiran et al., 2018). Compensation for the loading effect requires information on the temporal and spatial variability of aerosol properties. Drinovec et al. (2015) have suggested a real-time loading effect compensation algorithm that uses a dual-point approach in which the incoming flow is divided into two streams with different rates and passing through two sample points. Therefore, two synchronous measurements of ATN may be obtained, both of which are affected by different loading effects. These techniques have been incorporated into the new Aethalometer, which is used in this work.

2.3. Methodology

2.3.1. Calculation of absorption Ångström exponent

The calculation of the absorption Ångström exponent involves a power law dependence of σ_{abs} on λ. This relationship is commonly expressed as:

$$\sigma_{abs}(\lambda) = K\lambda^{-\alpha}, \quad (1)$$

where σ_{abs} is the spectrally dependent absorption coefficient, λ is the light wavelength, and K is a constant. The absorption Ångström exponent is represented by α, which may then be calculated from measured σ_{abs} as a function of different wavelengths following the formula:

$$\alpha_{\lambda_1\text{-}\lambda_2} = -\frac{\ln(\sigma_{abs,\lambda_1} / \sigma_{abs,\lambda_2})}{\ln(\lambda_1 / \lambda_2)}. \quad (1)$$

2.3.2. Aethalometer model

The Aethalometer model is based on the work of Sandradewi et al. (2008) and aims to quantify the contribution of fossil fuel (BC_{ff}) and biomass burning (BC_{bb}) to the total BC mass concentration. It assumes that the aerosol optical absorption coefficient can be viewed as the sum of fossil fuel and biomass combustion fractions. The two sources exhibit specific Ångström exponents with respect to aerosol absorption because BC from fossil fuels has a weak wavelength-dependence, while BC originating from biomass burning exhibits enhanced absorption towards shorter wavelengths, and thus the sources of these two components can be modeled (Drinovec et al., 2015; Herich et al., 2011). Following a study by Kirchstetter et al. (2004), the absorption Ångström exponents of fossil fuels (α_{ff} = 1) and biomass burning (α_{bb} = 2) were used in this study. The quantification of BC from fossil fuels and biomass burning may then be calculated by solving equations (3–7).

$$\sigma_{\text{abs}}(\lambda) = \sigma_{\text{abs}}(\lambda)_{\text{ff}} + \sigma_{\text{abs}}(\lambda)_{\text{bb}} \quad (3)$$

In equation (3), $\sigma_{\text{abs}}(\lambda)_{\text{ff}}$ and $\sigma_{\text{abs}}(\lambda)_{\text{bb}}$ refer to the aerosol absorption coefficient of BC from the combustion of fossil fuels and biomass burning at a wavelength λ, respectively. Furthermore,

$$\frac{\sigma_{\text{abs}}(370)_{\text{ff}}}{\sigma_{\text{abs}}(880)_{\text{ff}}} = \left(\frac{370}{880}\right)^{-\alpha_{\text{ff}}} \quad (4)$$

$$\frac{\sigma_{\text{abs}}(370)_{\text{bb}}}{\sigma_{\text{abs}}(880)_{\text{bb}}} = \left(\frac{370}{880}\right)^{-\alpha_{\text{bb}}} \quad (5)$$

$$\text{BC}_{\text{ff}} = \text{BC}\frac{\sigma_{\text{abs}}(880)_{\text{ff}}}{\sigma_{\text{abs}}(880)} \quad (6)$$

$$\text{BC} = \text{BC}_{\text{ff}} + \text{BC}_{\text{bb}} \quad (7)$$

2.3.3. HYSPLIT model

Air mass backward trajectories arriving at Nanjing were calculated using the United States National Oceanic and Atmospheric Administration (NOAA) Air

Resource Lab (ARL) Hybrid Single Particle Lagrangian Integrated Trajectory version 4.0 (HYSPLIT-4) model and the meteorological data derived from the Global Data Assimilation System (GDAS). Four-day backward air trajectories were computed at 500 m above ground level and 1-h time intervals. As this arrival altitude was suitable for the identification of long-range transport impacts, it ensured that the computation of the back-trajectories began within the heights of atmospheric boundary layer (Karaca et al., 2009).

2.3.4. PSCF and CWT models

The potential source contribution function (PSCF) model is a method of identifying source areas based on air trajectory analysis. It can localize suspected air pollutant source areas efficiently by counting air back-trajectory segment endpoints that terminate within each cell (Cheng et al., 2006; Dimitriou and Kassomenos, 2016). The PSCF value of a single grid cell (0.5°×0.5°) is given by the following equation:

$$\mathrm{PSCF}_{ij} = \frac{m_{ij}}{n_{ij}} \tag{8}$$

where n_{ij} is the total number of trajectory points that fall in the ijth cell and m_{ij} is the number of trajectory points included in the ijth cell, corresponding to trajectories with pollutant concentrations higher than a threshold value (Wang et al., 2009; Kong et al., 2013).

To overcome limitations with the PSCF, we further performed the concentration weighted trajectory (CWT) method to identify the source strengths of BC in Nanjing. In the CWT method, we used a plugin called TrajStat: GIS based software to elaborate the analysis which can be found elsewhere (Wang et al., 2009). In the CWT method, each grid cell is assigned a weighted concentration by averaging the sample concentrations that have associated trajectories crossing that grid cell represented as follows:

$$CWT = \frac{1}{\sum_{i=1}^{M} T_{ijl}} \sum_{i=1}^{M} C_l T_{ijl} \tag{9}$$

where CWT is the weighted concentration of BC in trajectory in the ijth cell, l and M

denote the trajectory indices and total number of trajectories, respectively. C_l is the concentration of BC observed at receptor site on arrival of trajectory l and T_{ijl} is the residential time of trajectory l in the ijth cell. Higher the value of CWT represents the magnitude of source strength associated with BC concentration observed at receptor site.

3. Results and discussion

3.1. General meteorology

Figure 2 shows the monthly variations of temperature (T), RH, precipitation (PP), and wind speed (WS) measured from the AWS during the years between 2015 and 2016 in the northern suburb of Nanjing. The monthly mean RH found higher than 60% during the observation period, and the highest value of 87% was occurred in October 2016. Whereas, total annual precipitation was measured of ~1350 mm, with an occurrence of maximum precipitation (~900 mm) was observed during summer (JJA months) and autumn (SON) seasons, which accounted for more than 70% of the total precipitation. An annual precipitation of 1687 mm noticed in 2016 which is at an increase of 65% compared to 2015. However, the ambient air temperature presented a distinct seasonal pattern, with the highest values (24–29ºC) in summer and the lowest values (3–7ºC) in winter (DJF months). A weak seasonal variation in WS was depicted in Nanjing, but the values were higher (1.8–2.4 m/s) during spring (MAM) and lower in winter (1.5–2.0 m/s).

3.2. Temporal variations in BC concentrations

The daily and monthly variations in the mass concentrations of BC from 2015 to 2016 are shown in Figure 3a. The daily averaged BC concentration measured at Nanjing varied from 150 ng/m^3 to10423 ng/m^3, with a mean value of 2200 ± 1309 ng/m^3 during the entire study period. In general, higher BC concentrations were mainly observed during December and January, with the monthly mean values fluctuating between 2796 ± 1646 ng/m^{3}and 3470 ± 2450 ng/m^3. The concentrations were relatively lower during other months, particularly in April and May, with the mean values were ranged between 933 ± 536 ng/m^{3}and 2778 ± 1486 ng/m^3. The maximum monthly mean concentrations of BC occurred in January of 2015, likely

caused by the occurrence of several severe pollution days during January 3–5, January 10, and January 24, when the daily averaged BC concentrations exceeded 5000 ng/m^3. The inter-annual variations in BC concentrations were observed in Nanjing. In 2015, the annual mean concentration of BC was 2654±1364 ng/m^3, while a lower mean value of 1866±1160 ng/m^3 was found in 2016. This decrease was mainly due to the occurrence of heavy precipitation in 2016 (Fig. 2), which indicates that the meteorological conditions played a crucial role in the variation of BC.

BC concentrations in Nanjing exhibited a substantial seasonal heterogeneity during the measurement period (Fig. 3b). The mean concentrations of BC by season in 2015 were found to be: spring = 2146 ± 938ng/m^3, summer = 2427 ±1217 ng/m^3, autumn = 2647 ± 1123 ng/m^3, and winter = 3454 ± 1790 ng/m^3. Mean while, BC concentrations for each season in 2016 were noticed as: spring = 1640 ± 1140 ng/m^3, summer = 1461 ± 744 ng/m^3, autumn = 1586 ± 773 ng/m^3, and winter = 2852 ± 1297 ng/m^3. The concentrations of BC were remained lower during spring and summer seasons likely related to the strong convective activity and heavy summer precipitation phenomena over the region (Kang et al., 2016). High BC concentrations in winter were mainly attributable to the severe emissions of anthropogenic pollutants produced more from the heating sources and the stability of the atmospheric boundary layer (ABL) due to lower temperature, which favored the accumulation of pollutants in the surface (Cao et al., 2009). Additionally, as the winters were dominated by westerly winds, air masses from inland areas may be expected to have been anthropogenically perturbed during their migration before reaching the sampling site, resulting in an increase in the BC concentration (Feng et al., 2014; Prasad et al., 2018). Similar results have also been observed for Shanghai (Zha et al., 2014), Hefei (Zhang et al., 2015), and Xi'an (Cao et al., 2009) over China; and Dhanbad (Singh et al., 2015), Kadapa (Begam et al., 2016), Gadanki (Ravi Kiran et al., 2018), and Pune (Kolhe et al., 2019) over India.

The variations of atmospheric aerosols are largely influenced by regional environmental conditions, including rural and urban settings. For example, the characteristics of aerosols may vary greatly due to different sources and atmospheric conditions. To facilitate a more holistic understanding of the distribution

characteristics of BC in different areas, Table 1 lists the observed BC concentrations from other sites. Overall, BC concentrations at urban sites were higher than those at rural, suburban, and remote sites. The BC concentration in the northern suburb of Nanjing was much lower than those at urban sites, such as Shenzhen (Huang et al., 2012) and Shenyang (Wang et al., 2011) in China, and at Delhi in India (Tiwari et al., 2013). However, it was comparable with urban Shanghai (Zha et al., 2014), suburban Beijing (Yan et al., 2008), and urban Pune in India (Kolhe et al., 2019). Furthermore, it was higher than the measurements over the outskirts of Lanzhou in China (Zhang et al., 2011), urban El Paso in the USA (Raysoni et al., 2011), urban Pune (Kolhe et al., 2019), and rural Évora in Portugal (Pereira et al., 2012), and lower than urban Granada (Valenzuela et al., 2017).

3.3. Diurnal variations in BC concentration

Figure 4 shows the diurnal variations of hourly averaged BC measured in the northern suburban area of Nanjing. The diurnal pattern of BC concentration exhibited a bimodal distribution with two peaks evident clearly in all the four seasons, which is similar to that observed in all sites listed in Table 1. The BC mass concentration was found maximum in the morning from 06:00 to 09:00 local time (LT). Then the mean value of BC began to decrease after 9:00 LT and reached its lowest values in the afternoon hours between 13:00 and 15:00 LT. The lowest mean BC concentration was approximately $3/5^{th}$ of the value observed in the morning. After 15:00 LT, the mean concentration of BC began to rise in the evening and remained elevated during the hours 19:00–22:00 LT, when it then decreased again until 04:00 LT of the following morning.

The highest BC concentrations were occurred in the morning and late evening hours mainly attributable to the severe emissions of pollutants from transportation sources during the morning and evening rush hours of traffic (Kumar et al., 2011; Zhang et al., 2015; Begam et al., 2016; Prasad et al., 2018). Meanwhile, the concentrations are also dependent upon the dynamics of the ABL height, which is usually stable during the early morning and late nighttime (Stull, 1998). The low value of BC in the afternoon might be related to strong atmospheric mixing and dilution of pollutants due to the

elevated ABL height, which increases with enhanced solar radiation (Kompalli et al., 2014). After sunset, BC concentrations began to rise and showed another moderate peak at midnight, which is due to vehicular exhausts and anthropogenic emissions. Besides, the decrease in the surface temperature can cause temperature inversion, and hence the formation of a stable nocturnal ABL in which pollutants are bound in the shallow ABL (Aruna et al., 2013). It is interesting to note that the peak and valley of BC concentration during winter occurred at 09:00 and 15:00 LT, respectively, which is 2–3 h later than during the other three seasons. This could be explained by the delay of local human activities because of the cold weather (Cao et al., 2009).

3.4. Source apportionment of BC

The absorption Ångström exponent (α) has typically been used to describe the spectral dependence of light absorption for aerosols derived from different sources and with different absorption characteristics to study and understand its spectral dependence. For BC, α was less than 1.0 when aerosols produced from the combustion of fossil fuels; while aerosols emitted from biomass burning, it showed stronger spectral dependence in absorption characteristics with high values (~1.8) and those mixed with dust exhibited much more higher α (>2). This clearly shows that the values of α derived in this study are consistent and close to that found in the works of Kirchstetter et al. (2004), hence followed the same.

The monthly mean variations in α over Nanjing is illustrated in Figure 5a. It is found that α showed greater than 1.0 during the entire observation period, without any obvious seasonal change. The monthly mean of α in 2015 exhibited a wide range of fluctuations, with a maximum value of 1.45 occurred in January and minimum (0.99) in July. The variation in monthly mean α in 2016 was mild, with a range of 1.14–1.30. The annual mean α in 2015 and 2016 were found 1.26 and 1.18, respectively, which indicates that BC aerosols over Nanjing mainly originated from fossil fuel combustion. From the seasonal frequency distribution of α shown in Fig. 5a, it can be seen that the spring and winter seasons were characterized by high α levels with a median value of 1.25, while the median value decreased to 1.19 during autumn. However, the

343 percentage of high values (α>1.6） during autumn accounted for 11% of the total,
344 signifies the frequent occurrence of substantial biomass burning events to clear the
345 agricultural waste from the farmlands in Nanjing. The α level in summer was slightly
346 lower than during other seasons, with a median value of 1.1. However, α ranged from
347 0.8 to1.8, implies that the effect of biomass burning on BC concentrations during
348 summer and autumn seasons cannot be ignored relative to the BC sources from fossil
349 fuel combustion which is at a greater extent as observed in this study.

350 In order to have more intuitively comprehend for the relative contributions of
351 fossil fuel (ff) and biomass burning (bb) to BC concentration in different seasons, the
352 monthly mean values of BC_{ff}, $BC_{bb,}$ and their percentage contributions were
353 calculated using the Aethalometer model (Sandradewi et al., 2008). It is evident that
354 the mean contributions of BC_{ff} (BC_{ff}%) and BC_{bb}(BC_{bb}%) to the total BC were found
355 as ~81% and ~19%, respectively (Figure 5b). The maximum contribution from the
356 BC_{ff}% occurred in July 2015 (85%) and the minimum during January 2015 (73%).
357 Conversely, the contribution of BC_{bb} reached it's maximum in January 2015 (27%)
358 and minimum in July 2015 (15%). However, BC_{ff}, and BC_{bb} exhibited similar trends,
359 with higher values during winter Although, the values of BC_{bb} were similar (e.g., in
360 December 2016, June 2015, and October 2015) and, the BC_{bb}% in December 2016
361 was much lower than in the other two months due to the high BC concentration in
362 winter.

363 Similar to the seasonal pattern of α, the frequency distribution of BC_{bb}% also
364 exhibited noticeable seasonality (Figure. 5c). The overall contribution of BC_{bb}% was
365 comparatively lower during summer and the values mostly ranged between 10% and
366 17%, indicates that fewer biomass burning events occurred at the observation site or
367 that there was less contribution of such sources produced or transported from other
368 areas. However, the BC_{bb}% was centralized around 20% during spring and winter
369 seasons, suggesting that the contribution of biomass burning increased except, for the
370 existing fossil fuel emissions.

371 ***3.5. Analysis of BC transport from the CWT model***

372 Figure 7 presents the results obtained from the calculation of CWT model using

the HYSPLIT trajectories and GDAS meteorological achieved datasets for BC concentration in different seasons of Nanjing during the entire study period. The seasonal variation of airflow trajectory was obvious, and the potential source areas and their contributions were distinct in different seasons. Despite a large number of airmass trajectories originated from the East China sea due to the transport of ship emissions during spring, summer and fall seasons, their contribution to BC was small (< 2500 ng/m^3). However, the larger value of CWT with more contribution to BC (2500-5500 ng/m^3) in spring mainly distributed in the central parts of Anhui and western Zhejiang Provinces. In addition, the airflow from northern Fujian to eastern Jiangxi also contributed about 5000 ng/m^3 to BC. The larger value of CWT in summer occurred in the junction area between western Zhejiang and southern Anhui and contributed between 2500 and 3500 ng/m^3 to BC mass concentration. The BC concentration was lower in summer because of the greater influence of ocean air masses resulting in a larger amount of precipitation with high wind speed, which is also conducive to the diffusion of pollutants. In fall, the high value of CWT distributed from northern Jiangxi to southern Anhui Provinces, and northeastern Henan to western Shandong Provinces, which contributed more than 4000 ng/m^3 to the BC concentration. This is possibly attributed to the anthropogenic activities such as biomass combustion that occurred to clear the agricultural waste burning after harvesting in these areas during the fall season. The high CWT values in winter were mainly distributed in provinces of Fujian, Zhejiang, Jiangxi, Hubei and most areas of Anhui, contributing about 4500-6500 ng/m^3 to the BC mass concentration in Nanjing. The high CWT values with a large amount of BC (3000-4500 ng/m^3) were also distributed in parts of Henan and Shandong provinces possibly related to the biomass burning and heating in the north of China.

3.6. BC pollution events – A case study

To further understand the impacts of different sources on local BC concentrations, two BC pollution events were analyzed in this study. BC pollution events were defined as the periods when the daily averaged BC concentration exceeded the seasonal geometric mean concentration plus 1 time the standard deviation of the mean

(Cao et al., 2009). The selected BC events occurred during October 13–17 (event I) and December 20–23 of 2015(event II). Both the temperature and RH showed obvious diurnal variations during the event I (Fig. 6a), wherein the temperature reached its minimum before daybreak and its maximum in the afternoon, which was opposite to the pattern observed for RH. The time series of BC increased and decreased by a wide margin, with an average value of ~4800 ng/m^3 during event I. The hourly BC concentration sharply increased from 23:00 LT on October 13, and reached its maximum of 12063 ng/m^3 at 01:00 LT on October 14, before decreasing to 5530 ng/m^3 at 03:00 LT. Thereafter, the BC concentration continued to rise, reaching another maximum at 08:00 LT on the same day. Similar pattern was also observed from 23:00 LT on October 14 to 05:00 LT on the 15th October and from 21:00 LT on October 15 to 06:00 LT on the 16th October. In the event I, the contribution of BC_{bb} was nearly agreement with the variation of BC, with an average of 26%. This value was apparently higher than the mean BC_{bb}% of 19% during the observation period, which illustrates that biomass combustion made an important contribution to the high concentration of BC.

During event II (Fig. 6b), there was no evident regularity in T or RH. Two weak rainfall events occurred from 04:00–20:00 LT on December 20 and from 03:00–19:00 LT on the 22nd December and the cumulative precipitation values were 0.4 mm and 0.3 mm, respectively. Accordingly, the RH remained high for the duration of the event, with a mean value of 84%. Weak precipitation does not have an effective scavenging effect on pollutants, and the high RH in the near-surface layer was conducive to the accumulation of water vapor and pollutants. The mean concentration of BC was ~5230 ng/m^3 and was relatively stable during event II. An abrupt increase could be seen between 05:00 and 11:00 LT on December 21, wherein the highest BC concentration occurred at 09:00 LT on the 21st December, with a value of 12050 ng/m^3. The BC_{bb}% in event II was lower than in the event I. The averaged values of BC_{bb}% and BC_{ff}% were found to be 16% and 84%, respectively, which indicates that BC concentration during event II was mainly derived from the combustion of fossil fuels. It is further evident from the PSCF results (Figure S2 of SM) conducted during

both BC pollution events revealed that the potential sources originating from the northern Zhejiang, Jiangsu, and Anhui Provinces contributing more to the BC concentration observed at Nanjing.

4. Conclusions

Two years (2015-2016) of continuous and real-time data of BC mass concentrations were measured with a seven channel Aethalometer (AE-33) at a suburban site over Nanjing in the YRD region, East China. Along with the meteorology datasets, the observed BC concentrations have been used to analyze its temporal evolution, identify potential emission source areas and strengths (PSCF and CWT models), and also quantify their emission strengths of BC through apportionment model. During the entire study period, the mean BC concentration was found of 2200±1309 ng/m^3 and varied within the range 150–10423 ng/m^3. The monthly and seasonal variations of BC concentrations revealed high values during the winter, moderate in the autumn, and low in the spring and summer seasons. The BC mass concentration was found to exhibit a well-defined diurnal variation with two peaks between 06:00 and 09:00 LT and 19:00 and 22:00 LT in all the four seasons. This diurnal pattern is strongly associated with the dynamical behavior of the ABL height, meteorological conditions, and local anthropogenic emissions. The mean absorption Ångström exponent (α) during the entire study period was found to be ~1.21, with higher values being observed in spring and winter, and lower values found in summer. The contribution of BC_{ff} (BC_{ff} %) was dominated during the entire observation period, with the mean contributions of BC_{ff} % and BC_{bb}% to the total BC were approximately 81% and 19%, respectively Similar to α, BC_{bb}% also exhibited higher levels in spring and winter, and a lower level in summer, suggests an enhanced contribution from biomass burning sources except, for the existing fossil fuel emissions during spring and winter seasons. The results of the CWT model obtained for all seasons revealed that the northern Zhejiang and Anhui provinces were the important source regions for the transport of BC resulted in the high BC concentrations. This is consistent with the PSCF method conducted during the BC pollution events observed at Nanjing.

Acknowledgments and funding sources: This work was supported by the National Key Research and Development Program (2016YFC0203501), the National Natural Science Foundation of China (91544229 and 41775154), Six Talent Peaks Project of Jiangsu Province (JNHB-057 and JNHB-087), Major Project of Industry-University-Research Collaborative Innovation in Guangzhou（2016201604030082), Guangzhou Science and Technology Project（201604016053) and the Qing Lan Project. We acknowledge the work team of the China Meteorological Administration (CMA) meteorology observation station for maintaining the observation instrument.

Conflict of interests

The authors declare no conflict of interest.

References

An, J., Zhu, B., Wang, H., Li, Y., Lin, X., Yang, H., 2014. Characteristics and source apportionment of VOCs measured in an industrial area of Nanjing, Yangtze River Delta, China. Atmospheric Environment 97, 206-214.

Aruna, K., Kumar, T.V.L., Rao, D.N., Murthy, B.V.K., Babu, S.S., Moorthy, K.K., 2013. Black carbon aerosols in a tropical semi-urban coastal environment: Effects of boundary layer dynamics and long range transport. Journal of Atmospheric and Solar-Terrestrial Physics 104, 116-125.

Babu, S.S., Moorthy, K.K., 2002. Aerosol black carbon over a tropical coastal station in India. Geophysical Research Letters 29, 13-11-13-14.

Beegum, S.N., Moorthy, K.K., Babu, S.S., Satheesh, S.K., Vinoj, V., Badarinath, K.V.S., Safai, P.D., Devara, P.C.S., Singh, S.N., et al., 2009. Spatial distribution of aerosol black carbon over India during premonsoon season. Atmospheric Environment 43, 1071-1078.

Begam, G.R., Vachaspati, C.V., Ahammed, Y.N., Kumar, K.R., Babu, S.S., Reddy, R.R., 2016. Measurement and analysis of black carbon aerosols over a tropical semi-arid station in Kadapa, India. Atmospheric Research 171, 77-91.

Bisht, D.S., Dumka, U.C., Kaskaoutis, D.G., Srivastava, A.K., Soni, V.K., Attri, S.D., Sateesh, M., Tiwari, S., 2015. Carbonaceous aerosols and pollutants over Delhi urban environment: Temporal evolution, source apportionment and radiative forcing. Science of the Total Environment 521-522, 431-445.

Bond, T.C., 2004. A technology-based global inventory of black and organic carbon emissions from combustion. Journal of Geophysical Research 109.

Cao, J.J., Zhu, C.S., Chow, J.C., Watson, J.G., Han, Y.M., Wang, G.h., Shen, Z.X., An, Z.S., 2009. Black carbon relationships with emissions and meteorology in Xi'an, China. Atmospheric Research 94, 194-202.

Cheng, Y., Lee, S.C., Ho, K.F., Wang, Y.Q., Cao, J.J., Chow, J.C., Watson, J.G., 2006. Black carbon measurement in a coastal area of south China. Journal of Geophysical Research 111.

Dimitriou, K., Kassomenos, P., 2016. Combining AOT, Angstrom Exponent and PM concentration data, with PSCF model, to distinguish fine and coarse aerosol intrusions in Southern France. Atmospheric Research 172-173, 74-82.

Dimitriou, K., Kassomenos, P. 2014. Indicators reflecting local and transboundary sources of $PM_{2.5}$, and PM_{COARSE} in Rome - impacts in air quality. Atmospheric Environment, 96(7), 154-162.

Drinovec, L., Močnik, G., Zotter, P., Prévôt, A.S.H., Ruckstuhl, C., Coz, E., Rupakheti, M., Sciare, J., Müller, T., Wiedensohler, A., Hansen, A.D.A., 2015. The "dual-spot" Aethalometer: an improved measurement of aerosol black carbon with real-time loading compensation. Atmospheric Measurement Techniques 8, 1965-1979.

Dumka, U.C., Moorthy, K.K., Kumar, R., Hegde, P., Sagar, R., Pant, P., Singh, N., Babu, S.S., 2010. Characteristics of aerosol black carbon mass concentration over a high altitude location in the Central Himalayas from multi-year measurements. Atmospheric Research 96, 510-521.

Feng, J., Zhong, M., Xu, B., Du, Y., Wu, M., Wang, H., Chen, C., 2014. Concentrations, seasonal and diurnal variations of black carbon in $PM_{2.5}$ in Shanghai, China. Atmospheric Research 147-148, 1-9.

Hansen, A. D. A., Rosen, H., & Novakov, T. 1984. The aethalometer an instrument for the real-time measurement of optical absorption by aerosol particles. Science of the Total Environment, 36(JUN), 191-196.

Herich, H., Hueglin, C., Buchmann, B., 2011. A 2.5 year's source apportionment study of black carbon from wood burning and fossil fuel combustion at urban and rural sites in Switzerland. Atmospheric Measurement Techniques 4, 1409-1420.

Huang, X.F., Sun, T.L., Zeng, L.W., Yu, G.H., Luan, S.J., 2012. Black carbon aerosol characterization in a coastal city in South China using a single particle soot photometer. Atmospheric Environment 51, 21-28.

Joshi, H., Naja, M., Singh, K.P., Kumar, R., Bhardwaj, P., Babu, S.S., Satheesh, S.K., Moorthy, K.K., Chandola, H.C., 2016. Investigations of aerosol black carbon from a semi-urban site in the Indo-Gangetic Plain region. Atmospheric Environment 125, 346-359.

Karaca, F., Anil, I., & Alagha, O. 2009. Long-range potential source contributions of episodic aerosol events to pm profile of a megacity. Atmospheric Environment, 43(36), 5713-5722.

Kirchstetter, T.W., Novakov, T., Hobbs, P.V., 2004. Evidence that the spectral dependence of light absorption by aerosols is affected by organic carbon. Journal of Geophysical Research Atmospheres. 109 (D21), 1729–1742.

Kolhe, A.R., Ralegankar, S.D., Safai, P.D., Aher, G.R., 2019. Absorption properties of black carbon aerosols over environmentally distinct locations in south-western India: Temporal, spectral characterization and source apportionment. Journal of Atmospheric and Solar Terrestrial Physics 189, 1-17.

Kompalli, S.K., Babu, S.S., Moorthy, K.K., Manoj, M.R., Kumar, N.V.P.K., Shaeb, K.H.B., Joshi, A.K., 2014. Aerosol black carbon characteristics over Central India: Temporal variation and its dependence on mixed layer height. Atmospheric Research 147-148, 27-37.

Kong, X., He, W., Qin, N., He, Q., Yang, B., Ouyang, H., Wang, Q., Xu, F., 2013. Comparison of transport pathways and potential sources of PM10 in two cities around a large Chinese lake using the modified trajectory analysis. Atmospheric Research 122, 284-297.

Kumar, K.R., Narasimhulu, K., Balakrishnaiah, G., Reddy, B.S.K., Gopal, K.R., et al., 2011. Characterization of aerosol black carbon over a tropical semi-arid region of Anantapur, India. Atmospheric Research 100, 12-27.

Liu, Y., Yan, C., Zheng, M., 2018. Source apportionment of black carbon during winter in Beijing. Science of the Total Environment 618, 531-541.

Lyamani, H., Olmo, F.J., Foyo, I., Alados-Arboledas, L., 2011. Black carbon aerosols over an urban area in south-eastern Spain: Changes detected after the 2008 economic crisis. Atmospheric Environment 45, 6423-6432.

Pan, X.L., Kanaya, Y., Wang, Z.F., Liu, Y., Pochanart, P., Akimoto, H., Sun, Y.L., Dong, H.B., Li, J., Irie, H., Takigawa, M., 2011. Correlation of black carbon aerosol and carbon monoxide in the high-altitude environment of Mt. Huang in Eastern China. Atmospheric Chemistry and Physics 11, 9735-9747.

Pereira, S.N., Wagner, F., Silva, A.M., 2012. Long term black carbon measurements in the southwestern Iberia Peninsula. Atmospheric Environment 57, 63-71.

Prasad, P. Raman, M.R., Ratnam, M.V., Chen, W.N., Rao, S.V.B., Gogoi, M.M., Kompalli, S.K. Kumar, K.S., Babu, S.S., 2018. Characterization of atmospheric black carbon over a semi-urban site of Southeast India: Local sources and long-range transport. Atmospheric Research 213, 411-421.

Ramanathan, V., & Carmichael, G. 2008. Global and regional climate changes due to black carbon. Nature Geoscience, 36(1), págs. 335-358.

Ran, L., Deng, Z.Z., Wang, P.C., Xia, X.A., 2016. Black carbon and wavelength-dependent aerosol absorption in the North China Plain based on two-year aethalometer measurements. Atmospheric Environment 142, 132-144.

Ravi Kiran, V., Talukdar, S., Ratnam, M.V., Jayaraman, A., 2018. Long-term observations of black carbon aerosol over a rural location in southern peninsular India: Role of dynamics and meteorology. Atmospheric Environment 189, 264-274.

Raysoni, A.U., Sarnat, J.A., Sarnat, S.E., Garcia, J.H., Holguin, F., Luevano, S.F., Li, W.W., 2011. Binational school-based monitoring of traffic-related air pollutants in El Paso, Texas (USA) and Ciudad Juarez, Chihuahua (Mexico). Environmental Pollution 159, 2476-2486.

Sandradewi, J., Prévôt, A. S. H., Szidat, S., Perron, N., Alfarra, M. R., & Lanz, V. A., et al. 2008. Using aerosol light absorption measurements for the quantitative determination of wood burning and traffic emission contributions to particulate matter. Environmental Science & Technology, 42(9), 3316-23.

Singh, S., Tiwari, S., Gond, D.P., Dumka, U.C., Bisht, D.S., Tiwari, S., Pandithurai, G., Sinha, A., 2015. Intra-seasonal variability of black carbon aerosols over a coal field area at Dhanbad, India. Atmospheric Research 161-162, 25-35.

Streets, D. G., Gupta, S., Waldhoff, S. T., Wang, M. Q., Bond, T. C., & Bo, Y. 2001. Black carbon emissions in China . Atmospheric Environment, 35(25), 4281-4296.

Stull, 1998. An Introduction to Boundary Layer Meteorology, Kluwer Academic Publishers, Dordrecht.

Tan, H., Liu, L., Fan, S., Li, F., Yin, Y., Cai, M., Chan, P.W., 2016. Aerosol optical properties and mixing state of black carbon in the Pearl River Delta, China. Atmospheric Environment 131, 196-208.

Tiwari, S., Srivastava, A.K., Bisht, D.S., Parmita, P., Srivastava, M.K., Attri, S.D., 2013. Diurnal and seasonal variations of black carbon and $PM_{2.5}$ over New Delhi, India: Influence of meteorology. Atmospheric Research 125-126, 50-62.

Udayasoorian, C., Jayabalakrishnan, R.M., Suguna, A.R., Gogoi, M.M., Suresh Babu, S., 2014. Aerosol black carbon characteristics over a high-altitude Western Ghats location in Southern India. Annales Geophysicae 32, 1361-1371.

Vaishya, A., Singh, P., Rastogi, S., Babu, S.S., 2017. Aerosol black carbon quantification in the central Indo-Gangetic Plain: Seasonal heterogeneity and source apportionment. Atmospheric Research 185, 13-21.

Valenzuela, A., Arola, A., Anton, M., Quirantes, A., Alados-Arboledas, L., 2017. Black carbon radiative forcing derived from AERONET measurements and models over an urban location in the southeastern Iberian Peninsula. Atmospheric Research 191, 44-56.

Virkkula, A., Mäkelä, T., Hillamo, R., Yli-Tuomi, T., Hirsikko, A., Hämeri, K., Koponen, I.K., 2007. A Simple Procedure for Correcting Loading Effects of Aethalometer Data. Journal of the Air & Waste Management Association 57, 1214-1222.

Wang, H., An, J., Cheng, M., Shen, L., Zhu, B., Li, Y., Wang, Y., Duan, Q., Sullivan, A., Xia, L., 2016. One year online measurements of water-soluble ions at the industrially polluted town of Nanjing, China: Sources, seasonal and diurnal variations. Chemosphere 148, 526-536.

Wang, Y.F., Ma, Y.J., Lu, Z.Y., Zhou, D.P., Liu, N.H., Zhang, Y.H., Hong, Y., 2011a. In situcontinuous observation of atmospheric black carbon aerosol mass concentration in Liaoning region. Research of Environmental Sciences 24 (10), 1088-1096(in Chinese).

Yan, P., Tang, J., Huang, J., Mao, J.T., Zhou, X.J., Liu, Q., Wang, Z.F., Zhou, H.G., 2008.The measurement of aerosol optical properties at a rural site in Northern China.Atmospheric Chemistry and Physics 8, 2229-2242.

Zha, S., Cheng, T., Tao, J., Zhang, R., Chen, J., Zhang, Y., Leng, C., Zhang, D., Du, J., 2014. Characteristics and relevant remote sources of black carbon aerosol in Shanghai. Atmospheric Research 135-136, 159-171.

Zhang, L., Zhang, L., Zhang, D.L., Zhao, S.Q., Huang, J.P., Zhang, W., Shi, J.S., 2011.Property of black carbon concentration over outskirts of Lanzhou, NorthwestChina. China Environmental Science 31 (8), 1248-1255 (in Chinese).

Zhang, X., Rao, R., Huang, Y., Mao, M., Berg, M.J., Sun, W., 2015. Black carbon aerosols in urban central China. Journal of Quantitative Spectroscopy and Radiative Transfer 150, 3-11.

Zhuang, B.L., Wang, T.J., Liu, J., Li, S., Xie, M., Yang, X.Q., Fu, C.B., Sun, J.N., Yin, C.Q., Liao, J.B., Zhu, J.L., Zhang, Y., 2014. Continuous measurement of black carbon aerosol in urban Nanjing of Yangtze River Delta, China. Atmospheric Environment 89, 415-424.

Table 1. Comparison of black carbon (BC) mass concentrations at different sampling sites.

location	Environment type	Study period	BC concentration (ng/m^3)	Citation
Nanjing (32°21'N,118°72'E)	Suburban	2015-2016	2200 ± 1309	Present study
Nanjing (32.05°N,118.78°E)	Urban	2012	4157 ± 2626	Zhuang et al. (2014)
Shanghai (31.18°N,121.30°E)	Urban	2011-2012	2330	Zha et al. (2014)
Hefei	Urban	2012-2013	3500 ± 2500	Zhang et al. (2015)
Shenzhen (22.60°N,113.97°E)	Urban	2009	6000	Huang et al. (2012)
Xianghe (39.80°N,116.96°E)	Rural	2013-2014	5390 ± 4440	Ran et al. (2016)
Beijing (40.39°N,117.07°E)	Suburban	2003-2005	2120 ± 1620	Yan et al. (2008)
Shenyang (41.77°N, 123.50°E)	Urban	2008-2009	6140	Wang et al. (2011a)
Lanzhou (35.57°N, 104.08°E)	Remote	2007-2009	1568	Zhang et al. (2011)
Delhi (28.35°N, 77.12°E)	Urban	2011	6700 ± 5700	Tiwari et al. (2013)
Kadapa (14.47°N, 78.82 °E)	Rural	2011-2012	2200 ± 780	Begam et al. (2016)
Dhanbad (23.47°N, 86.30 °E)	Urban	2012	6300 ± 2700	Singh et al. (2015)
Pune (18.53ºN, 73.8ºE)	Urban	2015-2016	1924 ± 750	Kolhe et al. (2019)
Gadanki	Rural	2008-2017	2200	Ravi Kiran et al. (2018)
Vijayawada	Suburban	2016	3440±2070	Prasad et al. (2018)
Granada (37.16°N, 3.58 °W)	Urban	2005-2008	3000 ± 1500	Lyamani et al. (2011)
El Paso	Urban	2008	230 - 2480	Raysoni et al. (2011)
Évora (38.57°N, 7.91 °W)	Rural	2007-2009	1300 ± 1200	Pereira et al. (2012)
Granada (37.168ºN, 3.608ºW)	Urban	2005-2012	2900 ± 900	Valenzuela et al. (2017)

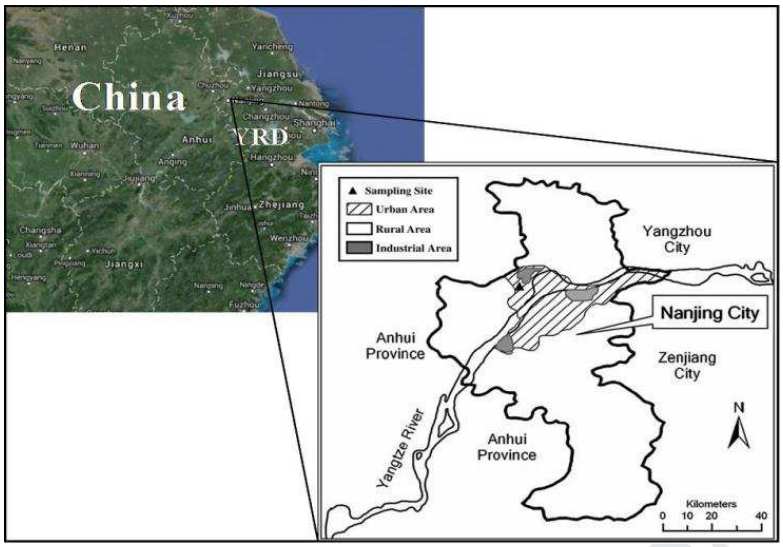

Figure 1. Geographical position of Nanjing city in the YRD region over Southeast China.

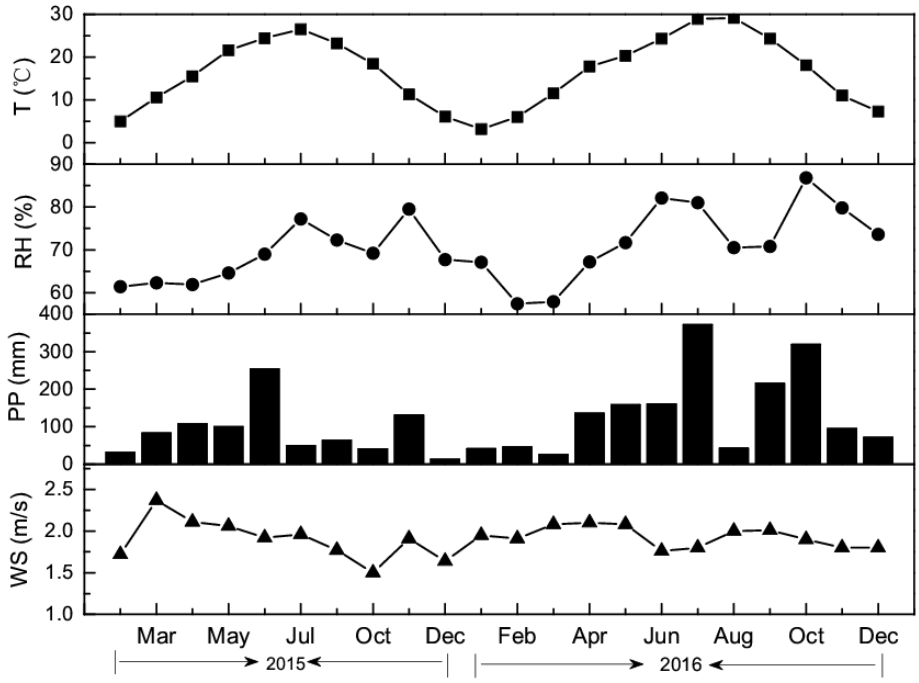

Figure 2. Monthly variations in temperature (T), relative humidity (RH), precipitation (PP) and wind speed (WS) during 2015-2016.

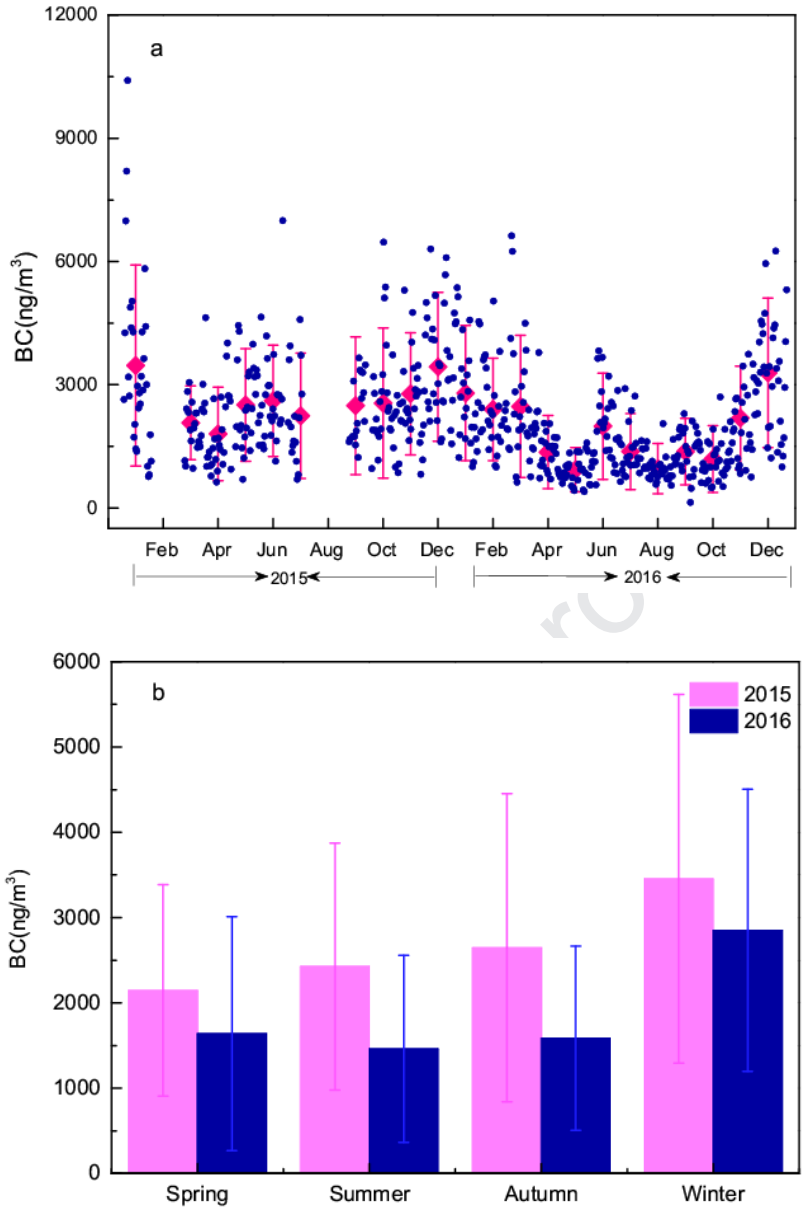

Figure 3. Daily (blue) and monthly (pink) variations of BC mass concentrations (a) and seasonal variations of BC mass concentrations (b) observed in Nanjing from January of 2015 to December of 2016.

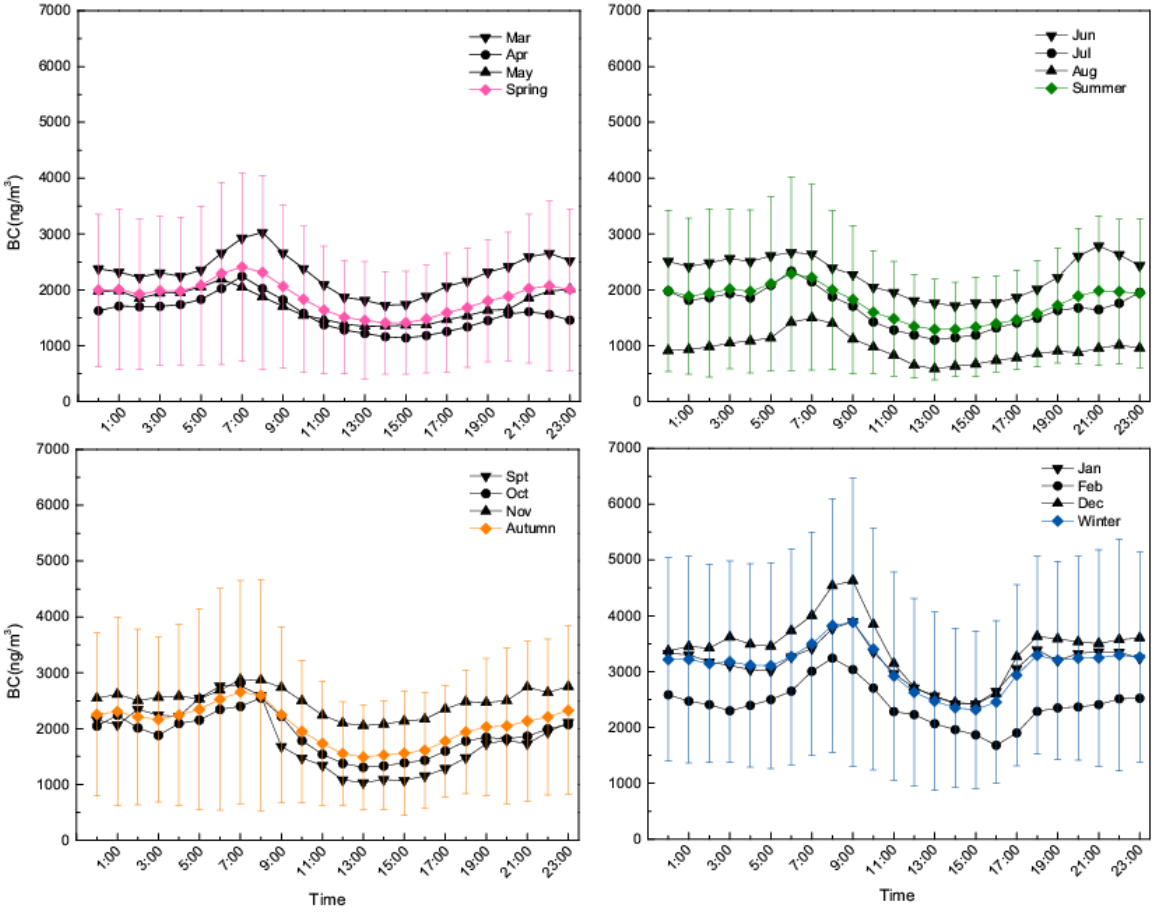

Figure 4. Diurnal variations of BC concentrations for different months and seasons during the entire study period. The solid lines corresponding to the dots denote the standard deviation.

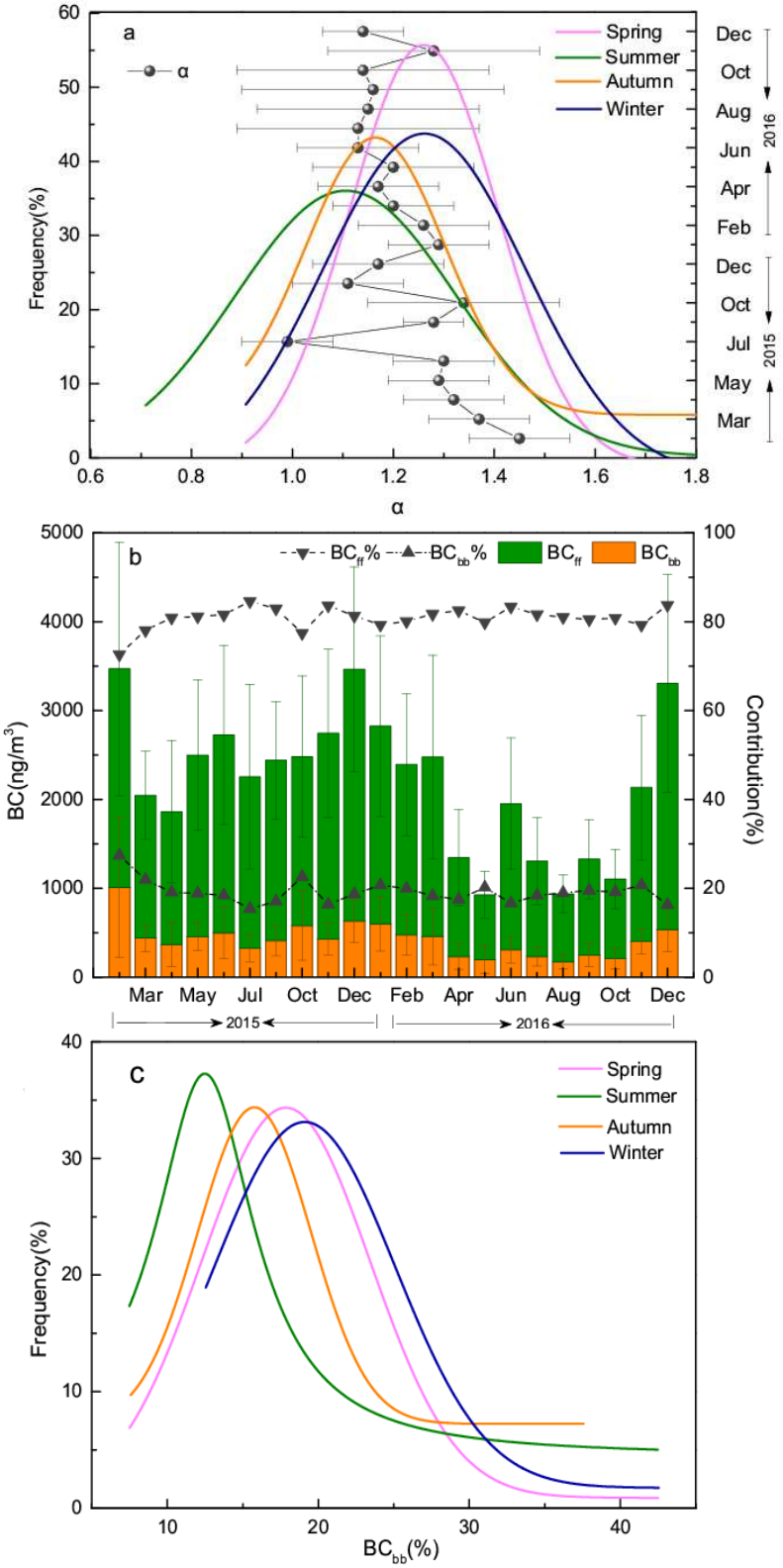

Figure 5. Monthly variations in the absorption Ångström exponent (α) and its frequency distributions for different seasons (a); monthly concentrations of BC from fossil fuels (BC_{ff}) and biomass burning (BC_{bb}) and their contributions in total BC (b); and seasonal frequency distribution of BC_{bb} (%) (c) observed over Nanjing.

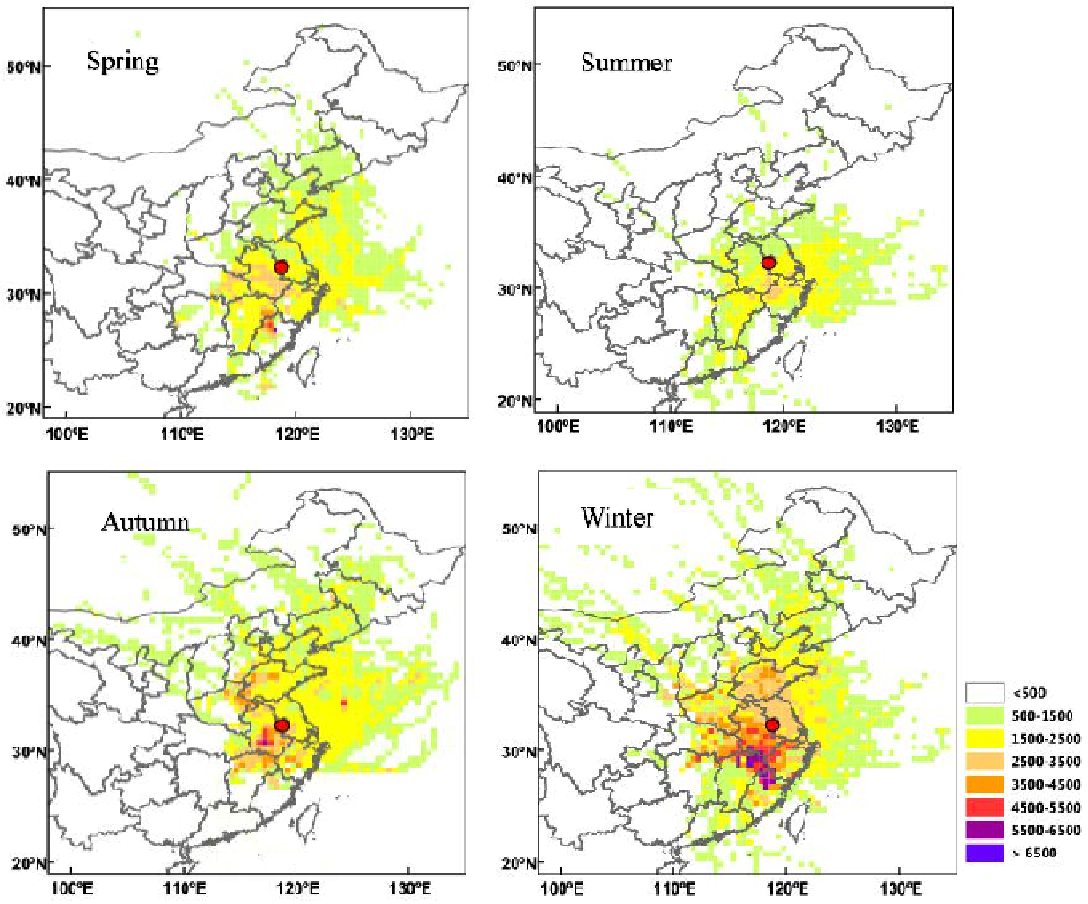

Figure 6. CWT model results obtained for different seasons presenting the long-range transport of BC concentration. The location of the measurement site is shown with the solid red circle.

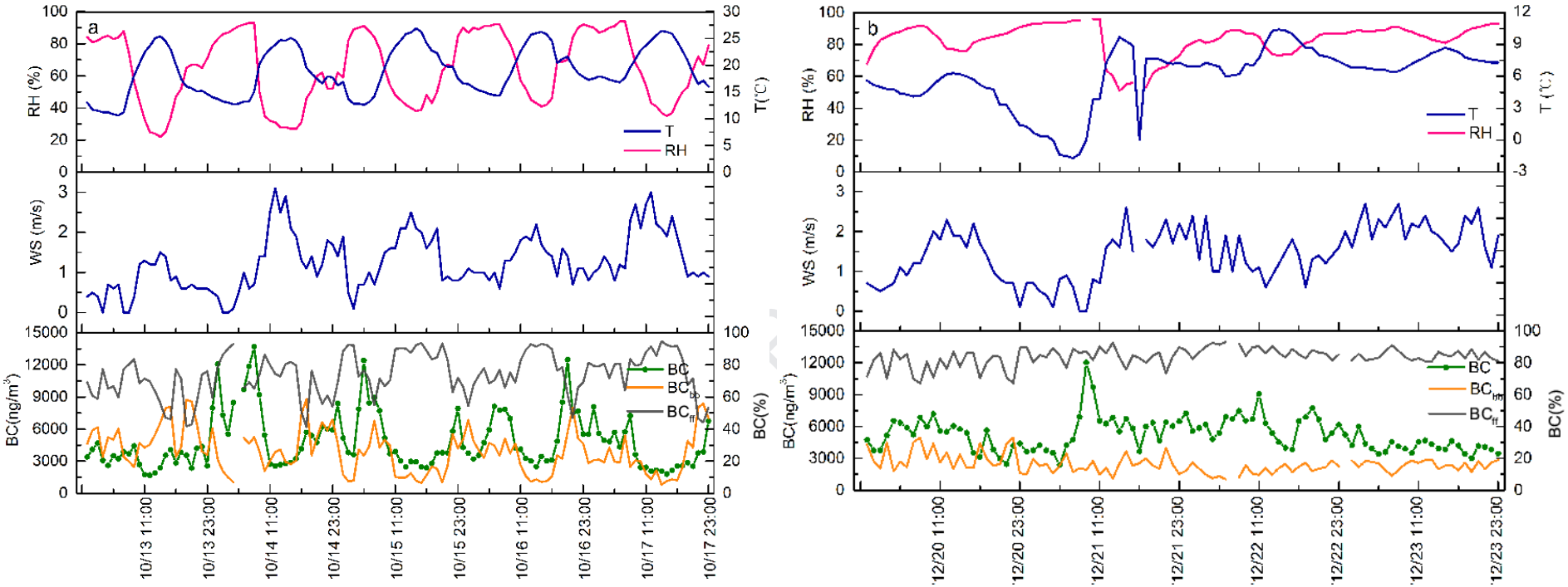

Figure 7. Time series of relative humidity (RH), temperature (T), wind speed (WS), BC mass concentration and the contributions of BCff (%) and BCbb (%) during event I (a) and event II (b) observed at Nanjing.

HIGHLIGHTS

1. Both seasonal and diurnal variations showed significant changes of BC mass concentration.
2. A strong BC aerosol absorption observed during spring and winter seasons attributed to fossil fuel and biomass combustion.
3. Fossil fuel emission was the major source of BC in Nanjing contributing 81% as evidenced from the source apportionment model.
4. CWT analysis revealed major potential sources of BC originating from Anhui and Zhejiang Provinces.